Negative-Valence Neurons in the Larval Zebrafish Pallium

Colton D. Smith[1,2], Zhuowei Du[1,3], William P. Dempsey[1], Scott E. Fraser[1,3,4,5], Thai V. Truong[1,3,4] and Don B. Arnold[1,4,5]

1. Department of Biological Sciences, Division of Molecular and Computational Biology, University of Southern California, Los Angeles, CA 90089
2. Neuroscience Graduate Program, University of Southern California, Los Angeles, CA 90089
3. Translational Imaging Center, University of Southern California, Los Angeles, CA 90089
4. Viterbi School of Engineering, University of Southern California, Los Angeles, CA 90089
5. Department of Quantitative and Computational Biology, University of Southern California, Los Angeles, CA 90089

Abstract:

An organism's survival depends on the rapid classification of sensory events as either harmful or beneficial. In mammals, this computation is partially performed by neurons in the amygdala that respond to signals with negative or positive valence. The larval zebrafish pallium is thought to contain homologs of the mammalian amygdala,

isocortex, and hippocampus; however, the signals encoded by pallial neurons remain largely uncharacterized. Using two-photon light-sheet microscopy to image 7–9-day-old zebrafish that express pan-neuronal GCaMP6s, we recorded calcium dynamics throughout the brain while presenting a panel of strongly aversive stimuli including infrared heat, electric shock, and a whole-field looming shadow, together with milder threats including vibration, loud sound, light transitions, and a partial looming stimulus. A compact cluster of neurons in the rostrolateral dorsal pallium (Rl) responded vigorously to strongly noxious and fully looming stimuli, but not to the milder cues. In contrast, neurons in the ventromedial pallium and habenula responded to all stimuli tested. Rl neurons are characterized by high *tiam2a* expression, suggesting they can be genetically accessed. Our results identify a dedicated negative valence locus in the teleost pallium and underscore the evolutionary conservation of valence coding circuits.

Introduction

To evaluate potential threats, organisms must predict future events based on sensory cues (Herberholz and Marquart, 2012). For example, when a predator approaches a fish, sudden changes in water pressure activate its lateral line system, which, combined with visual cues, allows it to predict that danger is imminent and swiftly evade the threat (Olszewski et al., 2012). How fish decide to flee, or, conversely, to mate or feed, remains poorly understood. In mammals, several lines of evidence suggest that this process involves the basolateral amygdala, where distinct ensembles encode negative and positive value (Beyeler et al., 2018; Grewe et al., 2017; Namburi et al., 2015; Tye, 2018; Xiu et al., 2014). Lesions or chemogenetic silencing of the amygdala blunt defensive behaviors and block fear conditioning (Bechara et al., 2003; Corder et al.,

2019; Downer, 1961; Feinstein et al., 2011; LeDoux et al., 1988; Phillips and LeDoux, 1992). The amygdala is also a locus of synaptic change following fear learning (Clem and Huganir, 2010; Goosens and Maren, 2002; Nabavi et al., 2014; Phillips and LeDoux, 1992; Quirk et al., 1995; Rogan et al., 1997). Finally, neurons in the basolateral amygdala project differentially depending on their valence, with negative-valence neurons projecting to the medial central amygdala and neighboring positive-valence neurons projecting to the nucleus accumbens, consistent with activation of the two sets of neurons causing distinct downstream effects (Beyeler et al., 2018; Fadok et al., 2017; Penzo et al., 2014; Tye et al., 2011).

The larval zebrafish (Danio rerio) is an excellent model system for studying sensory processing because its transparent brain is amenable to whole-brain imaging paradigms that require low scattering, such as selective plane illumination microscopy (SPIM; Ahrens et al., 2013). The high speed of SPIM and its low toxicity enable 4-D imaging across large areas of the larval zebrafish brain (Vladimirov et al., 2018). Furthermore, a modified SPIM that uses two-photon excitation (Truong et al., 2011) significantly reduces toxicity and increases penetration relative to 1-P SPIM. Although its brain is smaller and less complex than those of many other vertebrates, the zebrafish can, even in its larval stage, learn to modify responses to environmental stimuli (Gerlai, 2011). In particular, zebrafish are amenable to classical conditioning, which in some cases depends on distinct regions in the telencephalon (Lal et al., 2018; M Portavella et al., 2004; Portavella et al., 2002; Ruhl et al., 2015). Previously, we showed that a well-defined area in the rostrolateral pallium (Rl) contains neurons that respond to aversive

heating (Dempsey et al., 2022). Thus, RI in the zebrafish may play a similar role to that of the mammalian amygdala in calculating the valence of sensory stimuli. To test this hypothesis, we investigated whether neurons in RI respond specifically to negative-valence stimuli.

To characterize how neurons in the forebrain of a larval zebrafish respond to sensory stimuli of different valence, we mapped GCaMP (a genetically encoded Ca^{2+} indicator) fluorescence following exposure of the fish to stimuli ranging from highly threatening to mildly aversive. We found a tightly clustered group of neurons in RI that responded vigorously to negative-valence stimuli that are highly predictive of tissue damage, but not to less intense negative-valence stimuli. Two additional areas, the ventromedial pallium (Vm) and the habenula (Hb), contained neurons that responded to both types of stimuli. Negative-valence neurons in RI specifically expressed *tiam2a*, a homolog of a gene expressed in the mammalian hippocampus. Thus, we conclude that RI is a locus of threat assessment in the larval zebrafish brain containing negative-valence neurons that share a molecular marker with neurons in the mammalian hippocampus.

Results

Noxious stimuli activate pallial neurons

To investigate how neurons in the forebrain respond to negative-valence stimuli, we created a transgenic zebrafish line, Tg[CAG_{NRSE}:GCaMP6s], expressing GCaMP6s (Chen et al., 2013) driven by the chicken β-Actin CAG promoter (Quitschke et al., 1989) with an NRSE repressor element (Bergeron et al., 2012) added to diminish expression

in non-neuronal cells. Wholemount immunostaining for GCaMP6s and the neuronal marker HuC (elav3) in the forebrain of a 7 dpf Tg[CAG_{NRSE}:GCaMP6s] zebrafish shows almost complete overlap of the two labels, suggesting that virtually all neurons in the zebrafish pallium express GCaMP6s (**Fig. S1**). Note that some skin cells expressed GCaMP6s and were thus excluded from all analyses.

To explore the pallial responses to negative-valence stimuli in real time, we imaged the Tg[CAG_{NRSE}:GCaMP6s] zebrafish using a custom-built two-photon (2P) SPIM (Keomanee-Dizon et al., 2020) (**Fig. S2**). The 2P-SPIM microscope generates a 2P-excitation light sheet using ultrafast near-infrared laser pulses. This microscope combines non-linear excitation for high penetration depth with orthogonal light-sheet illumination for high acquisition speed and low photodamage (Truong et al., 2011). We immobilized 7–9 dpf fish by embedding them in agarose and placing them in a holder immediately adjacent to the SPIM's two objectives (**Fig. S2**).

In our initial studies, we exposed the fish to noxious infrared (IR) heating from a laser positioned over the zebrafish's right eye (**Figs. S2, 1A**), which we previously found elicited a strong escape response consisting of a tail flick (Dempsey et al., 2022). The IR stimulus consisted of a series of five 2-second pulses with 2-minute intervals between. Before, during, and after the stimulus, the SPIM imaged a series of optical sections at 11 depths spanning 60 mm, acquired sequentially every 0.12 seconds, completing a stack every 1.33 seconds. We found that three discrete areas in each hemisphere of the zebrafish forebrain showed an overall increase in fluorescence

114 (ΔF/F, see methods) in response to the IR stimulus (**Fig. 1B**). These areas correspond
115 to the left and right Hb (lHb and rHb), left and right RI (lRI and rRI), and left and right Vm
116 (lVm and rVm) (**Fig. S3**). Time-lapse images of fluorescent signals (with background
117 measured before the stimulus subtracted) show an abrupt increase shortly after the
118 stimulus, with average ΔF/F increasing significantly in each of the six areas (**Fig. 1C-E**,
119 n = 5 fish).
120
121 To characterize the response of pallial and habenular neurons more fully, we exposed
122 the fish to electric shock, another noxious stimulus. We used wires placed
123 approximately 1 mm from the otic vesicles (the ears) to deliver 500 mA of current for
124 400 ms (**Fig. 1F**). All six brain regions that increased activity with IR stimulation also
125 showed a qualitative increase in activity following the electric shock (**Fig. 1G, H**). In
126 addition, the average ΔF/F, measured after electric shock, was significantly higher than
127 measurements before the shock (n = 5 fish**, Fig. 1I, J**). These results show that the Hb,
128 RI, and Vm areas of the pallium bilaterally respond to two different noxious stimuli.
129
130 To better understand activity at the level of individual neurons, we used the Ca^{2+} signal
131 detection program CaImAn (Giovannucci et al., 2019) to extract neuronal responses
132 from the raw fluorescence data (see methods). Because the CaImAn program cannot
133 reliably distinguish signals from axons, dendrites, and somata, the signals may not
134 represent distinct cells; thus, we refer to the traces produced by CaImAn as "neuronal
135 components". We counted the number of neuronal components with averaged ΔF/F
136 responses that increased by 50% or more compared with before the stimulus, which we

137 refer to as "activated", and those that decreased by 50% or more, which we refer to as
138 "inhibited" (**Fig. 2A, B**). In response to IR heating, the ratio of activated to inhibited
139 neuronal components (A/I) was 5.0 for Hb, 2.0 for RI, and 4.8 for Vm (**Fig. 2C**).
140 Similarly, responses to electric shock had A/I ratios of 2.8 for Hb, 1.8 for RI, and 4.0 for
141 Vm (**Fig. 2D**).
142
143 Although it was not possible to expose the fish to multiple stimuli within a single imaging
144 session due to their fragility, we plotted the cumulative distribution of activated vs.
145 inhibited neuronal components onto a canonical fish template for both IR heating and
146 electric shock so that we could compare responses to the two stimuli (**Fig. 2C, D**). In RI,
147 components activated by both IR heating and electric shock were generally located in
148 the same region, caudal and medial to the region containing inhibited components.
149
150 **Distinct responses to full and partial looming stimuli in RI**
151 Given that two different noxious stimuli evoked activity in Hb, RI, and Vm (**Figs. 1, 2**),
152 we asked how the same regions would respond to a non-noxious stimulus that still
153 indicated an imminent threat of bodily harm. For many visual species, including
154 zebrafish, a looming stimulus consisting of a black disc that increases in size, mimicking
155 the shadow of an approaching predator, signals a potential threat and triggers
156 evolutionarily hard-wired defensive behaviors like freezing or fleeing (Neo et al., 2015).
157 To generate a looming stimulus, we projected a black disc onto a small projector screen
158 located to the right of the 7–9 dpf zebrafish, which started as a 1° point and grew over
159 500 ms to cover the fish's entire visual field. After remaining at full size for 5 s, the disc

contracted back to 1°. During this sequence, we monitored GCaMP fluorescence. Similar to exposure to IR heating and electric shock, the full looming stimulus immediately elicited increased activation in all six regions activated by noxious stimuli (**Fig. 3A**-**C**). There was residual activity in several areas, including rVm, rRl, and lRl 8 s after the stimulus ceased. Quantitation of the average ΔF/F before and after presentations showed significant increases in all six areas (n = 5, **Fig. 3D, E**).

Given the robust response to the full looming stimulus, we asked whether a similar, but less intense stimulus, might elicit a different neuronal response. Thus, we developed a partial looming stimulus, which is similar to the full looming stimulus, except the disc stops growing after 300 ms when it covers approximately 48 degrees of the visual field, and then, after 5 s, reduces in size over 300 ms to a 1° point, which could mimic a predator that comes close to the fish but then stops (**Fig. 3F**). Strikingly, the partial-looming stimulus did not elicit a significant overall ΔF/F increase in Rl, although increases in activity in Hb and Vm were significant (n = 7, **Fig. 3G**-**J**).

A/I ratios of individual activated and inhibited neuronal components responding to the full looming stimulus were 7.2 in Hb, 1.4 in Rl, and 5.5 in Vm, indicating that activation predominated overall (**Fig. 4A**, **C**). However, in response to the partial looming stimulus, neuronal components showed an A/I of 1.2 in Hb and 3.0 in Vm, whereas inhibited components predominated in Rl (A/I = 0.41; **Fig. 4B**, **D**). Thus, multiple measures of neuronal activity are consistent with Rl being activated by noxious stimuli and a full

182 looming stimulus, but not by a partial looming stimulus. In contrast, Vm and Hb are
183 activated by all stimuli tested.
184
185 **Mild negative-valence stimuli do not activate RI neurons.**
186 To further test whether RI neurons respond only to highly threatening stimuli, such as
187 noxious stimuli, or to a full looming stimulus, we exposed larval zebrafish to stimuli that
188 could be perceived as threatening but do not indicate imminent bodily harm and
189 measured the response in Hb, RI, and Vm. Specifically, we exposed the zebrafish to
190 sudden vibration, loud noises, and a transition from light to darkness. Each of these
191 stimuli has been shown to elicit startle responses, including C-bends, in larval zebrafish
192 (Beppi et al., 2021; Neo et al., 2015), consistent with their being inherently threatening
193 (Bartoszek et al., 2021). To expose the fish to vibration while recording GCaMP activity
194 with the SPIM, we tapped the right side of the imaging chamber with a plastic stick for 5
195 s. We also presented an auditory stimulus by sounding an airhorn that produced a 120-
196 130 dB sound lasting 0.5 s. Finally, fish that had been equilibrated to darkness, then
197 exposed to light for 4 s, followed by an abrupt return to darkness, were analyzed for
198 response to the light-to-dark transition. Each stimulus was repeated 5 times with a 2-
199 min interval between trials. During and after each stimulus, increased activity was
200 apparent in Hb and Vm, whereas no overall activity change was observed in RI (**Fig**.
201 **5A-I**).
202
203 Statistical analysis showed that overall $\Delta F/F$ increased significantly in the rHb, lVm, and
204 rVm in response to tapping, but activity in RI did not increase significantly (n = 6 fish,

205 **Fig. 6A, B**). Similar results were found for exposure to the air horn blast, where activity
206 significantly increased in Hb and Vm, but not in RI (n = 4, **Fig. 6C, D**). Finally, overall
207 ΔF/F increased significantly in rHb and lVm, but not in RI, following a dark-to-light
208 transition (n = 5, **Fig. 6E, F**). Consistent with these results, A/I ratios for the neuronal
209 components found in Hb and Vm ranged from 1.6-4.3 but were substantially less than 1
210 (0.29-0.66) in RI for tapping, airhorn, and light-to-dark transitions (**Fig. 7A-F**). Thus,
211 overall activity in Hb and Vm increases significantly in response to moderately
212 threatening stimuli, at least unilaterally, and activated neuronal components outnumber
213 those that are inhibited. In contrast, in RI, overall ΔF/F does not increase significantly,
214 and inhibited neuronal components outnumber activated ones.
215
216 In conclusion, our results suggest that RI responds exclusively to the most threatening
217 stimuli, but not to less threatening stimuli both in terms of overall activity and A/I ratio of
218 neuronal components (**Fig. 8**). In contrast, Hb and Vm respond at least unilaterally to all
219 negative-valence stimuli and neuronal components have A/I ratios > 1 (**Fig. 8**),
220 regardless of whether they are strongly or weakly threatening. Thus, in principle, signals
221 present in RI could be used to identify highly threatening stimuli.
222
223 **Tiam2a-positive neurons in the rostrolateral pallium.**
224 To better understand the properties of neurons in the RI area that respond specifically to
225 imminent threats, we used the MapZebrain cellular-resolution atlas of the larval
226 zebrafish brain (Kunst et al., 2019). We found that in 6 dpf transgenic fish (y264Et, see
227 methods), the *tiam2a* promoter drives GFP specifically in a region of the pallium that

228 matches the location of RI neurons. *tiam2a* is the zebrafish homolog of the mammalian
229 gene *Tiam2*, which encodes a Rac1-associated GEF and is expressed primarily in the
230 hippocampus (Chiu et al., 1999).
231
232 To test whether *tiam2a* expression is a marker for neurons that respond to threatening
233 stimuli, we exposed 7–9 dpf Tg[tiam2a:GFP] larval zebrafish to heating with an IR laser.
234 Then we performed wholemount immunocytochemistry to detect pERK, a marker of
235 neuronal activity. A projection image of GFP and pERK shows striking colocalization
236 between the two markers, with virtually every GFP+ neuron expressing pERK (**Fig. 9A,**
237 **B**)**.** In contrast, under control conditions with no noxious stimuli present, we observed
238 little pERK expression in GFP+ neurons (**Fig. 9C, D**). To quantify the amount of co-
239 expression between the two, we measured the total intensity of pERK labeling in cells
240 that expressed GFP and subtracted the background intensity of pERK labeling
241 measured in cells in a nearby region of the fish brain that did not express *tiam2a*. pERK
242 labeling in GFP+ cells was ~20-fold higher in the IR Laser exposed group (n = 6) than in
243 the control group (n = 8), a statistically significant difference (one-tailed t-test; **Fig 9E**).
244 These data are consistent with *tiam2a* being a marker for pallial neurons that are more
245 active when zebrafish are exposed to noxious stimuli.
246
247 To investigate the morphology of RI neurons, we examined Tg[tiam2a:GFP] fish (**Fig.**
248 **9F**). From the dorsal view, GFP-labeled neurons are highly clustered in RI, and from the
249 coronal view, they appear superficial and dorsal. Furthermore, they have short axons,
250 suggesting they are involved in local connectivity. Thus, *tiam2a* promoter-mediated

expression defines a tightly packed group of neurons that respond to a noxious stimulus in the 7–9 dpf larval zebrafish. These neurons are likely negative-valence neurons that respond specifically to a variety of stimuli, indicating a high likelihood of bodily injury, but not to less threatening aversive stimuli.

Discussion

In this study, we defined responses of neurons in the larval zebrafish forebrain to noxious stimuli (IR heating and electric shock), non-noxious threatening stimuli (full looming), and less threatening stimuli (partial looming, vibration, loud noise, and dark-to-light transitions). Prior research has shown that in the adult zebrafish, neurons in the pallial area DI, which partially overlaps with RI, drive ongoing habenular activity (Bartoszek et al., 2021). However, dynamic responses of forebrain neurons to negative-valence stimuli have not been reported previously. Here, we have found that noxious and non-noxious threatening stimuli activate a distinct population of tightly clustered neurons within the rostrolateral dorsal pallium (RI). However, neurons within this same region do not respond to less threatening stimuli. In contrast, neurons in the ventromedial pallium and the habenula respond to all the stimuli tested, encompassing both highly threatening and mildly aversive stimuli.

In addition to neuronal components activated by negative-valence stimuli, we found components in RI that exhibited reduced activity upon exposure to noxious and threatening stimuli. Previously, it was found that neurons inhibited by negative-valence stimuli may also be activated by positive valence stimuli, suggesting that these neurons

may respond to positive valence (Belova et al., 2008; Smith and Torregrossa, 2021). The ratio of activated to inhibited neuronal components was highly correlated with whether the overall signal from a given region increased in response to a specific stimulus. A/I ratio (number of activated vs. inhibited neuronal components) > 1 was correlated with regional activation, whereas A/I < 1 was associated with a lack of activation. In the future, it will be important to test positive-valence stimuli to determine whether they elicit responses in neurons inhibited by negative-valence stimuli. Attempts in this study to elicit a response from forebrain neurons to the smell of food, a positive-valence stimulus, were unsuccessful (data not shown). Additionally, it will be important to determine whether individual neurons in Vm and Hb are broadly tuned to negative-valence stimuli or respond to stimuli of all valences.

It is important to emphasize that RI neurons respond to both looming and noxious stimuli. For cells to be classified as negative-valence, they must respond not only to inherently painful stimuli but also to stimuli that are potentially threatening (Pignatelli & Beyeler, 2018). We found that a full-coverage looming shadow activated rostrolateral neurons, along with ventromedial and habenular regions, similarly to physically noxious stimuli. However, a partial looming shadow failed to elicit a response in RI, although it activated Hb and Vm. Interestingly, it has been shown that when a zebrafish is exposed to a full looming stimulus that covers all of the visual field, it is likely to freeze, whereas a fish exposed to a looming disc that stops growing when the visual field is only partially covered (**Fig. 3F**), is more likely to try to escape (Temizer et al., 2015). Thus, results from this paper suggest that signals from RI, which responds differentially to full and

297 partial looming stimuli, may contribute to the initiation of appropriate defensive
298 behaviors in response to threats.
299
300 In this study, we exploited the unique properties of the larval zebrafish to obtain parallel
301 recordings of neuronal activity throughout the forebrain in response to negative-valence
302 stimuli. One drawback of using larval zebrafish is that they are relatively delicate,
303 making it difficult to present multiple stimuli to the same fish. Consequently, although it
304 is possible to conclude that neurons in RI are likely to respond when the fish is exposed
305 to one of several different stimuli, we cannot conclude that individual neurons respond
306 to more than one stimulus. In addition, it was difficult to relate the stimuli to behavioral
307 responses. Although tail flicks and heart rate were monitored with every response (not
308 shown), there were no uniform responses to specific stimuli. However, electric shock
309 (Kenney et al., 2017; Manuel et al., 2014), looming stimulus (Temizer et al., 2015),
310 vibration (Eaton et al., 2001), loud noise (Eaton et al., 2001; Neo et al., 2015), dark-to-
311 light and light-to-dark transitions (Beppi et al., 2021) all provoked escape behavior when
312 zebrafish were exposed to them in other contexts. It is possible that being encased in
313 agarose, a requirement for SPIM, limited the fish's behavioral responses. In our
314 experiments, and perhaps for agarose-encased zebrafish in other contexts, neural
315 signatures of negative-valence stimuli are stronger and more consistent than behavioral
316 ones. These findings suggest that forebrain activity, particularly in RI, might be a better
317 indicator of the internal state of the zebrafish's brain than behavior. Together, our results
318 suggest that a transgenic zebrafish expressing GCaMP under the *tiam2a* promoter
319 could provide real-time insight into the animal's internal state.

320

321 Several studies have suggested that the dorsomedial pallium in teleost fish, including
322 zebrafish, is the homolog of the amygdala and the dorsolateral pallium is homologous to
323 the hippocampus based on developmental, topological, and molecular arguments
324 (Baker and Wong, 2021; Mueller et al., 2011; von Trotha et al., 2014). In addition, the
325 medial pallium in general and a specific type of pallial neuron were found to be
326 necessary for fear conditioning in zebrafish (Broglio et al., 2005; Lal et al., 2018; Manuel
327 Portavella et al., 2004; Portavella et al., 2002). In contrast, the results from this study
328 and our previous study suggest that RI neurons are similar in some respects to neurons
329 in the mammalian amygdala. For instance, both of our studies show that RI neurons
330 respond to negative-valence stimuli, a response also seen in many neurons in the
331 mammalian amygdala (Beyeler et al., 2018). RI neurons also become responsive to
332 neutral stimuli following a novel form of classical conditioning (Dempsey et al, 2022).
333 Similarly, following fear conditioning, neurons in the mammalian amygdala become
334 responsive to conditioned stimuli that were paired with unconditioned stimuli (Grewe et
335 al., 2017; Zhang and Li, 2018). Finally, neurons within RI exhibit an increase in
336 excitatory synapses following classical conditioning, and amygdalar neurons undergo
337 long term potentiation, consistent with synaptic change, following fear conditioning
338 (Rogan et al., 1997). However, unlike the amygdala, where negative- and positive-
339 valence neurons are distributed in a salt and pepper fashion (Beyeler et al., 2018), the
340 negative-valence cells that we found in RI tend to be tightly clustered (**Fig. 9**).
341 Furthermore, *tiam2a* is a homolog of mammalian *Tiam2*, which is primarily expressed in
342 the hippocampus, and is less abundant in the amygdala (Chiu et al., 1999). Thus, our

data suggest that RI shares attributes of both the amygdala and the hippocampus, and that teleost fish may have unique brain structures with no exact homologs in mammals.

Author contributions: C.D.S. and D.B.A. designed the experiments and wrote the paper; C.D.S. performed the live-imaging research, contributed new analytic tools, and analyzed data; Z.D. performed the pERK experiments; T.V.T. and S.E.F. designed and built the SPIM used for live imaging. W.P.D. performed preliminary experiments that were critical for the development of the experimental protocols used in this paper. D.B.A. secured funding and supervised all aspects of the project.

Materials and Methods

Zebrafish husbandry and embryo/larval care

Many of the methods presented in this paper were developed previously (Dempsey et al., 2022). Larval and adult Casper mutant zebrafish were maintained in an in-house veterinary facility in accordance with protocols approved by the University of Southern California (USC) Institutional Animal Care and Use Committee (IACUC). All experiments described in this work were approved by the USC IACUC. Embryos were kept in egg water (1.19 g NaCl, 0.377 g CaSO4·2H2O, 265 mL methylene blue, filled up to 5 liters with ddH_2O) at 28 °C in an incubator with a 13 hr:11 hr light:dark cycle until 5-6 dpf, when they were transferred to tanks within the husbandry facility. On the husbandry system, zebrafish were also maintained on a 13 hr:11 hr light:dark cycle. The air and water temperature in the zebrafish facility are maintained at 26-28°C. Zebrafish larvae used in experiments (7–9 dpf) were transferred between the facility and the

366 experimental apparatus in zebrafish husbandry system water (H.S.W.) and kept at 26-
367 28°C between experiments.
368

369 **Tg[CAG$_{NRSE}$:GCaMP6s]**

370 To monitor cell Ca^{++} activity in these experiments, we used the transgenic zebrafish
371 Tg[CAG$_{NRSE}$:GCaMP6s] with GCaMP6s (Chen et al., 2013) expression driven by a β-
372 Actin promoter (Quitschke et al., 1989) to drive widespread expression and 3X NRSE
373 (neuron-restrictive silencer element) to restrict expression to neurons (Bergeron et al.,
374 2012).
375

376 **Tg[tiam2a:GFP]**

377 The transgenic fish y264Et (originally created by the lab of Harold Burgess), with the
378 construct Et(SCP1:GAL4FF), uniquely labels Tiam2a-positive cells with GFP within the
379 rostrolateral pallium (Sprague et al., 2003).

380 This transgenic fish was deposited in the ZFIN database (Ruzicka et al., 2015) with the
381 following citation: Marquart, G.D., Tabor, K.M., Brown, M., Strykowski, J.L., Varshney,
382 G.K., LaFave, M.C., Mueller, T., Burgess, S.H., Higashijima, S., and Burgess, H.A.
383 (2015) Enhancer Trap Transgenics. ZFIN Direct Data Submission. (http://zfin.org).

384 **Mounting Zebrafish in Caddie for Imaging on FlexSPIM**

385 To prepare for behavioral experiments, zebrafish subjects were first embedded in a
386 custom behavioral training caddie generated by Protolabs (Stereolithography, ABS-like
387 Translucent Clear [WaterShed]). Specs: ABS-Like Translucent Clear (WaterShed),
388 Normal Res, Natural, Stereolithography, X: 0.980in Y: 0.206in Z: 0.311in. The caddie is
389 filled with 200 mL of 1% (w/v) agarose, melting point ≤ 65°C (Millipore Sigma;
390 SeaPlaque, Cat:50101) dissolved in egg water containing methylene blue, which
391 suppresses fungal growth. During agarose embedding and fluorescence imaging
392 experiments, zebrafish were anesthetized in a final concentration of 70 ppm MS-222
393 (Western Chemical, Fluka analytical, Cat: A5040-100G) + 70 ppm Isoflurane (Phoenix
394 SKU 012ABB-250CC), an IACUC-approved combination that has been shown to enable
395 fast recovery from anesthesia as compared to using MS-222 alone (Huang WC*, et al.,*
396 2010). The anesthetics are dissolved in filter sterilized HSW. For all experiments
397 involving agarose- embedding of the zebrafish, a 1.5% (w/v) solution of low melting
398 point agarose (Sea Plaque Agarose, Lonza) dissolved in filter sterilized husbandry
399 system water consisting of instant ocean (ASIN: B000255NKA) and baking soda
400 dissolved in reverse osmosis water to achieve pH 7.2 and a conductance of ~700 μS)
401 with anesthetic is used. There was no bias in zebrafish gender for larval experiments,

402 as sex determination does not occur in zebrafish before the juvenile stage, ~24 dpf
403 (Uchida et al., 2002).
404
405 As the agarose solidifies (before it completely solidifies at 5 min), a hair stem (human
406 hair attached to a plastic rod) is used to position the zebrafish so that the body axis is
407 parallel to the surface of the chamber (normal swimming orientation). Once the agarose
408 solidifies, the caddie is placed into a 60 mm culture dish (Corning, Cat: 430166) and 10
409 ml of fresh filter-sterilized H.S.W. is added. The agarose is then shaved down with a
410 razor such that only the head and body are encased. Before the anesthetic wears off
411 after the introduction of the fresh H.S.W. solution (~30 seconds), the tail of the zebrafish
412 (just posterior to the swim bladder) is carefully freed from the agarose using fine forceps
413 (biology tip profile, Fine Science Tools, Cat: 11251-10). The rostral aspect of the
414 zebrafish (anterior to the swim bladder) is held firmly in place by the agarose. The
415 caddie is then transferred to another 60 mm culture dish in preparation for
416 transportation to the imaging room.

417 **FlexSPIM Light Sheet Microscope**

418 After the zebrafish has been mounted into the custom Protolabs caddie, it is ready to be
419 placed onto the flexSPIM. The flexSPIM is a versatile, multi-laser twin-microscope
420 system for light-sheet imaging designed and built for multiphoton and visible wavelength
421 fluorescence light sheet excitation (Keomanee-Dizon et al., 2020). The caddie is
422 securely fastened on the dive bar and placed into the chamber filled with 80 ml of fresh,
423 filter-sterilized H.S.W. During imaging, the objective position is programmed to follow a
424 saw waveform such that the objective takes a unidirectional path starting at the top of

the fish pallium (0 mm) and transitioning through to the most ventral aspect of pallium (60 mm) at a frequency of 0.75 Hz. The brain camera follows a square waveform that instructs it to acquire 11 images per objective cycle.

Arduino

For the behavioral experiments, an Arduino unit (Arduino UNO Rev3, Arduino.cc) and the software (Arduino software [IDE]) from the same company are used to control the stimuli. For the IR experiments, a simple program was designed to control the infrared laser (NIR RLCO-980-1000-F laser, Roithner Lasertechnik) by turning it on and off for two seconds, every two minutes. For the electricity experiments, a simple program was designed to allow the native Arduino 5V output to be turned on and off for 400 ms every two minutes.

Volumetric Visualization of Neural Activation

To visualize stimulus-evoked neural activation, volumetric calcium-imaging data were reconstructed into three-dimensional heat maps. Eleven consecutive image planes acquired with the flexSPIM immediately before stimulus onset were combined to generate a baseline 3D fluorescence volume. The same procedure was repeated for frames acquired after the stimulus (the specific time selected was within a 3 s post-stimulus window to capture the peak GCaMP response). The pre- and post-stimulus volumes were visualized side-by-side to illustrate regional activation patterns. Each 3D volume was rendered in coronal and dorsal orientations and manually curated to exclude superficial skin layers and non-neuronal regions, providing volumetric heat maps of GCaMP fluorescence before and after stimulation

Time-Lapse Analysis of Whole Regions

To quantify the temporal dynamics of stimulus-evoked activity within a region as a whole, time-lapse calcium-imaging data were analyzed from 90 consecutive frames acquired with the flexSPIM, with frame 45 corresponding to stimulus onset. Data from multiple trials were averaged to generate representative activation profiles for the left/right habenula, left/right rostrolateral regions, and left/right ventromedial regions of the brain. Using ImageJ, regions of interest were manually defined and the mean fluorescence intensity was measured across all frames, producing time-series traces of average neuronal activity before, during, and after each stimulus.

Calcium Imaging Data Processing and Spatial Registration

Time-series calcium-imaging data were processed using the open-source CaImAn package (Giovannucci *et al.*, 2019) to perform motion correction, signal extraction, and neuronal component identification. Rigid and non-rigid motion correction were applied to minimize motion artifacts and ensure accurate spatial alignment across frames. Following registration, a constrained non-negative matrix factorization (CNMF) model was applied, with key input parameters (e.g., expected neuron diameter, local-correlation threshold, and signal-to-noise cut-offs) empirically optimized to match the imaging resolution and fluorescence dynamics of the dataset. This optimization yielded spatial footprints and corresponding $\Delta F/F$ fluorescence traces for individual neuronal components. Model performance was iteratively evaluated through inspection of residual maps and assessment of spatial–temporal consistency.

Neuronal components were selected from anatomically defined regions and depths encompassing the habenula (~10 μm), rostrolateral region (~30 μm), and ventromedial region (~50 μm). Each region consisted of two bilaterally symmetric areas measuring approximately 50 μm × 50 μm. The habenula regions were located at the most caudal aspect of the brain, the rostrolateral regions were positioned rostrally and laterally, and the ventromedial regions were situated ventrally and medially, near the midline of the brain. Within each region, ΔF/F fluorescence traces were extracted for all identified neuronal components.

To correct for gradual fluorescence-intensity drift resulting from photobleaching, a rolling mean filter with a window size of 10 frames was applied to stabilize the ΔF/F time series. For each stimulus type, five trials were performed, except for the partial-looming stimulus, which was presented three times. For every trial, 44 frames preceding (~1min) and 45 frames following (~1min) the stimulus onset were extracted and averaged across trials, with frame 45 corresponding to the time of stimulus delivery. This procedure produced six averaged 90-frame time series per fish, corresponding to left and right hemispheric regions of the habenula, rostrolateral, and ventromedial areas.

To determine which neuronal components exhibited activation or inhibition in response to the stimulus, the mean ΔF/F values from frames 45–50 (post-stimulus window) were compared with the mean of the preceding 40 frames (baseline). Components showing ΔF/F ≥ +50% relative to baseline were classified as activated, while those with ΔF/F ≤ −50% were classified as inhibited.

Binary activation maps, showing activated and inhibited components for all fish and stimulus conditions were then registered onto a canonical template fish (three templates: habenula, rostrolateral, and vetromedial), with activated components represented in red and inhibited components in blue. The canonical template was constructed to represent an "ideal" reference fish and to standardize minor morphological variations across individuals. Registration parameters were manually ascertained using ITK-SNAP, using the midline and the skin-brain boundaries as anatomical landmarks. Using these parameters, each image analyzed was geometrically transformed (cropped, scaled, rotated, and translated) to align with the appropriate canonical template using custom Python scripts incorporating the libraries OpenCV, Matplotlib, and NumPy. The XY coordinates of activated and inhibited components were then extracted from the registered images and plotted onto the canonical template to generate composite activation/inhibition maps showing bilateral regional responses to each stimulus.

Heating Tg[tiam2a:GFP] Larval Zebrafish using an IR Laser (Figure 9)

Experimental procedures in this section were partially adapted from (Dempsey et al., 2022). To begin, Tg[tiam2a:GFP] zebrafish larvae were embedded in custom behavioral training molds: a 60 mm culture dish filled with 1% agarose dissolved in egg water, with a 10 mm diameter circle cut out from the center. The zebrafish was anesthetized and then embedded in the 10 mm diameter circle with 500 ml agarose + anesthetic (70 ppm MS-222 + 70 ppm Isoflurane (SKU 012ABB-250CC). While the agarose solidified, the zebrafish's position was parallel to the surface of the chamber, at the top of the agarose surface, and was maintained using a single bristle brush. After 5 min, 10 mL of sterilized

513 husbandry system water was added to the chamber. Using fine forceps, the tail of the
514 zebrafish was carefully freed from the agarose. All free-floating agarose was removed
515 from the dish. The dish was then positioned under the objective of a custom-built
516 behavioral microscope such that the right eye of the zebrafish was directly under where
517 the infrared laser spot would be when turned on (NIR RLCO-980-1000-F laser, Roithner
518 Lasertechnik). An Arduino was programmed to deliver the infrared heating laser for two
519 seconds, a total of ten times, with an intertrial separation of 2 minutes. After the fish
520 underwent ten trials, it was then fixed in PFA prior to pERK immunohistochemistry.
521

522 **pERK Immunohistochemistry**

523 After exposing 7–9 dpf Tg[tiam2a;GFP] larval zebrafish to the infrared laser ten times,
524 zebrafish were fixed in 4% PFA diluted in 1x PBS (pH 7.4), 70 ppm MS-222, 70 ppm
525 Isoflurane, covered in aluminum foil, and kept at 4°C overnight. Then, fish were washed
526 3 times in 1x PBS (pH 7.4) and 0.25% PBST (0.25% Triton X-100 in PBS). After 3x
527 PBST washes, the zebrafish were placed in 150 mM Tris HCl (pH 9) for 5 min at room
528 temperature, followed by 20 minutes at 65°C. Once this was complete, the samples
529 were cooled to room temperature and given 3x PBST washes. Zebrafish were then
530 permeabilized on ice for 45 minutes with 1x PBS, 0.05% Trypsin-EDTA (Sigma, T4049-
531 100ML) diluted in 1x PBS (pH 7.4). After another 3x PBST wash cycle, the zebrafish
532 were placed for 1 hour at room temperature in blocking buffer solution; (1x PBS, 1%
533 bovine serum albumin, 2% DMSO, 2% NGS, 0.25% Triton X-100. Zebrafish were
534 stained with primary rabbit anti-phosphorylated Erk1/2 antibodies at a 1:300 dilution
535 (Cell Signaling, Catalog #4696) in blocking buffer on a rotating platform at 4°C

536 overnight. After 5X PBST washes, the zebrafish were transferred to a blocking buffer
537 solution containing a 1:1000 dilution of Alexa Fluor 568-conjugated goat anti-rabbit
538 secondary antibody (Invitrogen, A-11011) and incubated overnight at 4°C on an orbital
539 shaker in the dark. After 5 PBST washes, samples were moved to PBS solution and
540 imaged on a Zeiss LSM 780 confocal (Translational Imaging Center, USC).
541

542 **Statistical Analysis**

543 Calcium signal curves and heatmaps were calculated using Python 3.12 scripts.
544 Statistical differences for pre- vs post-stimulus AUC values were assessed using one-
545 tailed, paired t-tests implemented in the SciPy library, and $p < 0.05$ was considered
546 statistically significant. No statistical methods were used to predetermine sample size.

547 **Experimental Setup and Stimulation Protocols for Neuronal Activity Imaging in**
548 **Fish**

549 All fish used in this study were given 90 min to acclimate on the flexSPIM system.
550 Following acclimation, each fish was imaged for 5 min to establish a baseline for
551 neuronal activity before being exposed to stimuli. The total duration of the experiments
552 was ~15-20 min. After the experiment was finished, the fish was released from the
553 agarose and allowed to rest in a dish for one hour. Only fish that were still alive and
554 healthy after this waiting time were included in the analysis.
555

556 **Near-Infrared laser**

557 Once the fish was prepared for imaging, it was positioned such that its right eye was hit
558 by the IR laser (NIR RLCO-980-1000-F laser, Roithner Lasertechnik). While imaging,

the IR laser was turned on for 2 seconds before being turned off. This was repeated 2 minutes later for a total of 5 trials.

Electric shock

Once the fish was prepared for imaging, two 1-pin dual-male jumper wires were secured onto the dive bar such that the pin connectors were positioned on or near both sides of the fish, where the body meets the tail. They were positioned such that when current is applied, it travels between the wires, creating a circuit with the fish in between, causing a small electric shock. While imaging, a 500 mA electric shock was administered to the zebrafish through electrodes connected to a 5 V Arduino pin for 400 ms. This was repeated every 2 minutes, for a total of 5 trials.

Full-looming Stimulus

Once the fish was prepped for imaging, a red-backlit projector screen was positioned on the right side of the fish. The window on the chamber covered 66° of the fish's visual field. A small black circle (1° of the fish's visual field) was maintained throughout the duration of the experiment. At the beginning of each trial, the spot was expanded until it fully covered the entire projection screen (1° to 66 degrees of the visual field) over 500 ms, hence the name "full-looming stimulus". Following 5 s, the stimulus returned to its original size. This was repeated 2 min later for a total of 5 trials.

Partial-looming stimulus

Once the fish was prepped for imaging, it was exposed to a stimulus similar to the full-looming stimulus, except that the black circle expanded to 48° over 300 ms, partially

covering the visual field. The black circle remained at 48° for 5 seconds before contracting back to its original size of 1° over 300 ms. This process was repeated 2 min later, for a total of 3 trials.

Tapping

During imaging, the experimenter tapped the side of the chamber with a plastic stick for 5 s. This process was repeated 2 min later, for a total of 5 trials.

Airhorn

While imaging, an air horn (1.4 oz, Betterboat) sounded a 120-130 dB blast approximately 1 inch above the chamber. The experimenter wore ear protection to prevent hearing damage. This procedure was repeated 2 minutes later, for a total of 5 trials.

Light

Once the fish was prepared for imaging, a red-backlit projector screen was positioned on the right side of the fish, making the light visible to the fish. A small, removable cardboard card was then placed between the fish and the projector, keeping the fish in complete darkness. During imaging, the card was removed for 5 s to expose the fish to light. After 5 seconds, the card was placed back between the fish and the projector to block the light. This procedure was repeated 2 minutes later, for a total of 5 trials.

Data Availability

Raw and processed data on Jupyter notebooks containing analysis pipelines are available on https://gin.g-node.org/coltonsm/Zebrafish_Valence_Project**.** The DOI for this repository will be made public upon being accepted for publication.

Acknowledgements

We thank M. Jones for microscopy technical support in the Translational Imaging Center, and L. Trinh and E. Carranza Lopez for zebrafish husbandry support. All microscopy was done at the Translational Imaging Center. This work was supported by the National Institute of Mental Health Grant 1UF1NS122082.

References

Ahrens MB, Orger MB, Robson DN, Li JM, Keller PJ. 2013. Whole-brain functional imaging at cellular resolution using light-sheet microscopy. *Nat Methods* **10**:413–420. doi:10.1038/nmeth.2434

Baker MR, Wong RY. 2021. Npas4a expression in the teleost forebrain is associated with stress coping style differences in fear learning. *Sci Rep* **11**. doi:10.1038/s41598-021-91495-7

Bartoszek EM, Ostenrath AM, Jetti SK, Serneels B, Mutlu AK, Chau KTP, Yaksi E. 2021. Ongoing habenular activity is driven by forebrain networks and modulated by olfactory stimuli. *Curr Biol* **31**:3861-3874 e3. doi:10.1016/j.cub.2021.08.021

Bechara A, Damasio H, Damasio AR. 2003. Role of the amygdala in decision-making. *Ann N Y Acad Sci* **985**:356–369. doi:10.1111/j.1749-6632.2003.tb07094.x

Belova MA, Paton JJ, Salzman CD. 2008. Moment-to-moment tracking of state value in the amygdala. *Journal of Neuroscience* **28**:10023–10030. doi:10.1523/JNEUROSCI.1400-08.2008

Beppi C, Beringer G, Straumann D, Bogli SY. 2021. Light-stimulus intensity modulates startle reflex habituation in larval zebrafish. *Sci Rep* **11**:22410. doi:10.1038/s41598-021-00535-9

633 Bergeron SA, Hannan MC, Codore H, Fero K, Li GH, Moak Z, Yokogawa T, Burgess
634 HA. 2012. Brain selective transgene expression in zebrafish using an NRSE
635 derived motif. *Front Neural Circuits* **6**:110. doi:10.3389/fncir.2012.00110
636 Beyeler A, Chang CJ, Silvestre M, Leveque C, Namburi P, Wildes CP, Tye KM. 2018.
637 Organization of Valence-Encoding and Projection-Defined Neurons in the
638 Basolateral Amygdala. *Cell Rep* **22**:905–918. doi:10.1016/j.celrep.2017.12.097
639 Broglio C, Gomez A, Duran E, Ocana FM, Jimenez-Moya F, Rodriguez F, Salas C.
640 2005. Hallmarks of a common forebrain vertebrate plan: specialized pallial areas
641 for spatial, temporal and emotional memory in actinopterygian fish. *Brain Res Bull*
642 **66**:277–281. doi:10.1016/j.brainresbull.2005.03.021
643 Chen TW, Wardill TJ, Sun Y, Pulver SR, Renninger SL, Baohan A, Schreiter ER, Kerr
644 RA, Orger MB, Jayaraman V, Looger LL, Svoboda K, Kim DS. 2013. Ultrasensitive
645 fluorescent proteins for imaging neuronal activity. *Nature* **499**:295–300.
646 doi:10.1038/nature12354
647 Chiu C-Y, Leng S, Martin KA, Kim E, Gorman S, Duhl DMJ. 1999. Cloning and
648 Characterization of T-Cell Lymphoma Invasion and Metastasis 2 (TIAM2), a Novel
649 Guanine Nucleotide Exchange Factor Related to TIAM1.
650 Clem RL, Huganir RL. 2010. Calcium-permeable AMPA receptor dynamics mediate fear
651 memory erasure. *Science (1979)* **330**:1108–1112. doi:10.1126/science.1195298
652 Corder G, Ahanonu B, Grewe BF, Wang D, Schnitzer MJ, Scherrer G. 2019. An
653 amygdalar neural ensemble that encodes the unpleasantness of pain. *Science*
654 *(1979)* **363**:276–281. doi:10.1126/science.aap8586
655 Dempsey WP, Du Z, Nadtochiy A, Smith CD, Czajkowski K, Andreev A, Robson DN, Li
656 JM, Applebaum S, Truong T V, Kesselman C, Fraser SE, Arnold DB. 2022.
657 Regional synapse gain and loss accompany memory formation in larval zebrafish.
658 *Proc Natl Acad Sci U S A* **119**. doi:10.1073/pnas.2107661119
659 Downer DJLD. 1961. CHANGES IN VISUAL GNOSTIC FUNCTIONS AND
660 EMOTIONAL BEHAVIOUR FOLLOWING UNILATERAL TEMPORAL POLE
661 DAMAGE IN THE "SPLIT-BRAIN" MONKEY, NATURE.
662 Eaton RC, Lee RK, Foreman MB. 2001. The Mauthner cell and other identified neurons
663 of the brainstem escape network of fish. *Prog Neurobiol* **63**:467–485.
664 doi:10.1016/s0301-0082(00)00047-2
665 Fadok JP, Krabbe S, Markovic M, Courtin J, Xu C, Massi L, Botta P, Bylund K, Müller C,
666 Kovacevic A, Tovote P, Lüthi A. 2017. A competitive inhibitory circuit for selection
667 of active and passive fear responses. *Nature* **542**:96–99. doi:10.1038/nature21047
668 Feinstein JS, Adolphs R, Damasio A, Tranel D. 2011. The human amygdala and the
669 induction and experience of fear. *Current Biology* **21**:34–38.
670 doi:10.1016/j.cub.2010.11.042
671 Gerlai R. 2011. Associative Learning in Zebrafish (Danio rerio), Methods in Cell Biology.
672 doi:10.1016/B978-0-12-387036-0.00012-8

673 Giovannucci A, Friedrich J, Gunn P, Kalfon J, Brown BL, Koay SA, Taxidis J, Najafi F,
674 Gauthier JL, Zhou PC, Khakh BS, Tank DW, Chklovskii DB, Pnevmatikakis EA.
675 2019. CaImAn an open source tool for scalable calcium imaging data analysis. *Elife*
676 **8**.
677 Goosens KA, Maren S. 2002. Long-term potentiation as a substrate for memory:
678 evidence from studies of amygdaloid plasticity and Pavlovian fear conditioning.
679 *Hippocampus* **12**:592–599. doi:10.1002/hipo.10099
680 Grewe BF, Grundemann J, Kitch LJ, Lecoq JA, Parker JG, Marshall JD, Larkin MC,
681 Jercog PE, Grenier F, Li JZ, Luthi A, Schnitzer MJ. 2017. Neural ensemble
682 dynamics underlying a long-term associative memory. *Nature* **543**:670–675.
683 doi:10.1038/nature21682
684 Herberholz J, Marquart GD. 2012. Decision Making and Behavioral Choice during
685 Predator Avoidance. *Front Neurosci* **6**:125. doi:10.3389/fnins.2012.00125
686 Kenney JW, Scott IC, Josselyn SA, Frankland PW. 2017. Contextual fear conditioning in
687 zebrafish. *Learn Mem* **24**:516–523. doi:10.1101/lm.045690.117
688 Keomanee-Dizon K, Fraser SE, Truong T V. 2020. A versatile, multi-laser twin-
689 microscope system for light-sheet imaging. *Review of Scientific Instruments* **91**.
690 Kunst M, Laurell E, Mokayes N, Kramer A, Kubo F, Fernandes AM, Forster D, Dal
691 Maschio M, Baier H. 2019. A Cellular-Resolution Atlas of the Larval Zebrafish
692 Brain. *Neuron* **103**:21-38 e5. doi:10.1016/j.neuron.2019.04.034
693 Lal P, Tanabe H, Suster ML, Ailani D, Kotani Y, Muto A, Itoh M, Iwasaki M, Wada H,
694 Yaksi E, Kawakami K. 2018. Identification of a neuronal population in the
695 telencephalon essential for fear conditioning in zebrafish. *BMC Biol* **16**:45.
696 doi:10.1186/s12915-018-0502-y
697 LeDoux JE, Iwata J, Cicchetti P, Reis DJ. 1988. Different projections of the central
698 amygdaloid nucleus mediate autonomic and behavioral correlates of conditioned
699 fear. *J Neurosci* **8**:2517–2529.
700 Manuel R, Gorissen M, Piza Roca C, Zethof J, Van De Vis H, Flik G, Van Den Bos R.
701 2014. Inhibitory avoidance learning in zebrafish (Danio Rerio): Effects of shock
702 intensity and unraveling differences in task performance. *Zebrafish* **11**:341–352.
703 doi:10.1089/zeb.2013.0970
704 Mueller T, Dong Z, Berberoglu MA, Guo S. 2011. The dorsal pallium in zebrafish, Danio
705 rerio (Cyprinidae, Teleostei). *Brain Res* **1381**:95–105.
706 doi:10.1016/j.brainres.2010.12.089
707 Nabavi S, Fox R, Proulx CD, Lin JY, Tsien RY, Malinow R. 2014. Engineering a
708 memory with LTD and LTP. *Nature* **511**:348–352. doi:10.1038/nature13294
709 Namburi P, Beyeler A, Yorozu S, Calhoon GG, Halbert SA, Wichmann R, Holden SS,
710 Mertens KL, Anahtar M, Felix-Ortiz AC, Wickersham IR, Gray JM, Tye KM. 2015. A
711 circuit mechanism for differentiating positive and negative associations. *Nature*
712 **520**:675–678. doi:10.1038/nature14366

Neo YY, Parie L, Bakker F, Snelderwaard P, Tudorache C, Schaaf M, Slabbekoorn H. 2015. Behavioral changes in response to sound exposure and no spatial avoidance of noisy conditions in captive zebrafish. *Front Behav Neurosci* **9**:28. doi:10.3389/fnbeh.2015.00028

Olszewski J, Haehnel M, Taguchi M, Liao JC. 2012. Zebrafish larvae exhibit rheotaxis and can escape a continuous suction source using their lateral line. *PLoS One* **7**. doi:10.1371/journal.pone.0036661

Penzo MA, Robert V, Li B. 2014. Fear conditioning potentiates synaptic transmission onto long-range projection neurons in the lateral subdivision of central amygdala. *Journal of Neuroscience* **34**:2432–2437. doi:10.1523/JNEUROSCI.4166-13.2014

Phillips RG, LeDoux JE. 1992. Differential contribution of amygdala and hippocampus to cued and contextual fear conditioning. *Behav Neurosci* **106**:274–285.

Portavella M, Torres B, Salas C. 2004. Avoidance response in goldfish: emotional and temporal involvement of medial and lateral telencephalic pallium. *J Neurosci* **24**:2335–2342. doi:10.1523/JNEUROSCI.4930-03.2004

Portavella Manuel, Torres B, Salas C. 2004. Avoidance Response in Goldfish: Emotional and Temporal Involvement of Medial and Lateral Telencephalic Pallium. *Journal of Neuroscience* **24**:2335–2342. doi:10.1523/JNEUROSCI.4930-03.2004

Portavella M, Vargas JP, Torres B, Salas C. 2002. The effects of telencephalic pallial lesions on spatial, temporal, and emotional learning in goldfish. *Brain Res Bull* **57**:397–399.

Quirk GJ, Repa C, LeDoux JE. 1995. Fear conditioning enhances short-latency auditory responses of lateral amygdala neurons: parallel recordings in the freely behaving rat. *Neuron* **15**:1029–1039.

Quitschke WW, Lin ZY, DePonti-Zilli L, Paterson BM. 1989. The β actin promoter. *Journal of Biological Chemistry* **264**:9539–9546. doi:10.1016/s0021-9258(18)60565-4

Rogan MT, Staubli U V, LeDoux JE. 1997. Fear conditioning induces associative long-term potentiation in the amygdala. *Nature* **390**:604–607. doi:10.1038/37601

Ruhl T, Moesbauer K, Oellers N, von der Emde G. 2015. The endocannabinoid system and associative learning and memory in zebrafish. *Behavioural Brain Research* **290**:61–69. doi:10.1016/j.bbr.2015.04.046

Ruzicka L, Bradford YM, Frazer K, Howe DG, Paddock H, Ramachandran S, Singer A, Toro S, Van Slyke CE, Eagle AE, Fashena D, Kalita P, Knight J, Mani P, Martin R, Moxon SAT, Pich C, Schaper K, Shao X, Westerfield M. 2015. ZFIN, The zebrafish model organism database: Updates and new directions. *Genesis* **53**:498–509. doi:10.1002/dvg.22868

Smith DM, Torregrossa MM. 2021. Valence encoding in the amygdala influences motivated behavior. *Behavioural Brain Research*. doi:10.1016/j.bbr.2021.113370

752 Sprague J, Clements D, Conlin T, Edwards P, Frazer K, Schaper K, Segerdell E, Song
753 P, Sprunger B, Westerfield M. 2003. The Zebrafish Information Network (ZFIN):
754 The zebrafish model organism database. *Nucleic Acids Res*.
755 doi:10.1093/nar/gkg027
756 Temizer I, Donovan JC, Baier H, Semmelhack JL. 2015. A Visual Pathway for Looming-
757 Evoked Escape in Larval Zebrafish. *Curr Biol* **25**:1823–1834.
758 doi:10.1016/j.cub.2015.06.002
759 Truong T V, Supatto W, Koos DS, Choi JM, Fraser SE. 2011. Deep and fast live
760 imaging with two-photon scanned light-sheet microscopy. *Nat Methods* **8**:757–760.
761 doi:10.1038/nmeth.1652
762 Tye KM. 2018. Neural Circuit Motifs in Valence Processing. *Neuron*.
763 doi:10.1016/j.neuron.2018.10.001
764 Tye KM, Prakash R, Kim SY, Fenno LE, Grosenick L, Zarabi H, Thompson KR,
765 Gradinaru V, Ramakrishnan C, Deisseroth K. 2011. Amygdala circuitry mediating
766 reversible and bidirectional control of anxiety. *Nature* **471**:358–362.
767 doi:10.1038/nature09820
768 Uchida D, Yamashita M, Kitano T, Iguchi T. 2002. Oocyte apoptosis during the
769 transition from ovary-like tissue to testes during sex differentiation of juvenile
770 zebrafish. *J Exp Biol* **205**:711–718.
771 Vladimirov N, Wang C, Höckendorf B, Pujala A, Tanimoto M, Mu Y, Yang CT,
772 Wittenbach JD, Freeman J, Preibisch S, Koyama M, Keller PJ, Ahrens MB. 2018.
773 Brain-wide circuit interrogation at the cellular level guided by online analysis of
774 neuronal function. *Nat Methods* **15**:1117–1125. doi:10.1038/s41592-018-0221-x
775 von Trotha JW, Vernier P, Bally-Cuif L. 2014. Emotions and motivated behavior
776 converge on an amygdala-like structure in the zebrafish. *European Journal of*
777 *Neuroscience* **40**:3302–3315. doi:10.1111/ejn.12692
778 Xiu J, Zhang Q, Zhou T, Zhou TT, Chen Y, Hu H. 2014. Visualizing an emotional
779 valence map in the limbic forebrain by TAI-FISH. *Nat Neurosci* **17**:1552–1559.
780 doi:10.1038/nn.3813
781 Zhang X, Li B. 2018. Population coding of valence in the basolateral amygdala. *Nat*
782 *Commun* **9**. doi:10.1038/s41467-018-07679-9
783

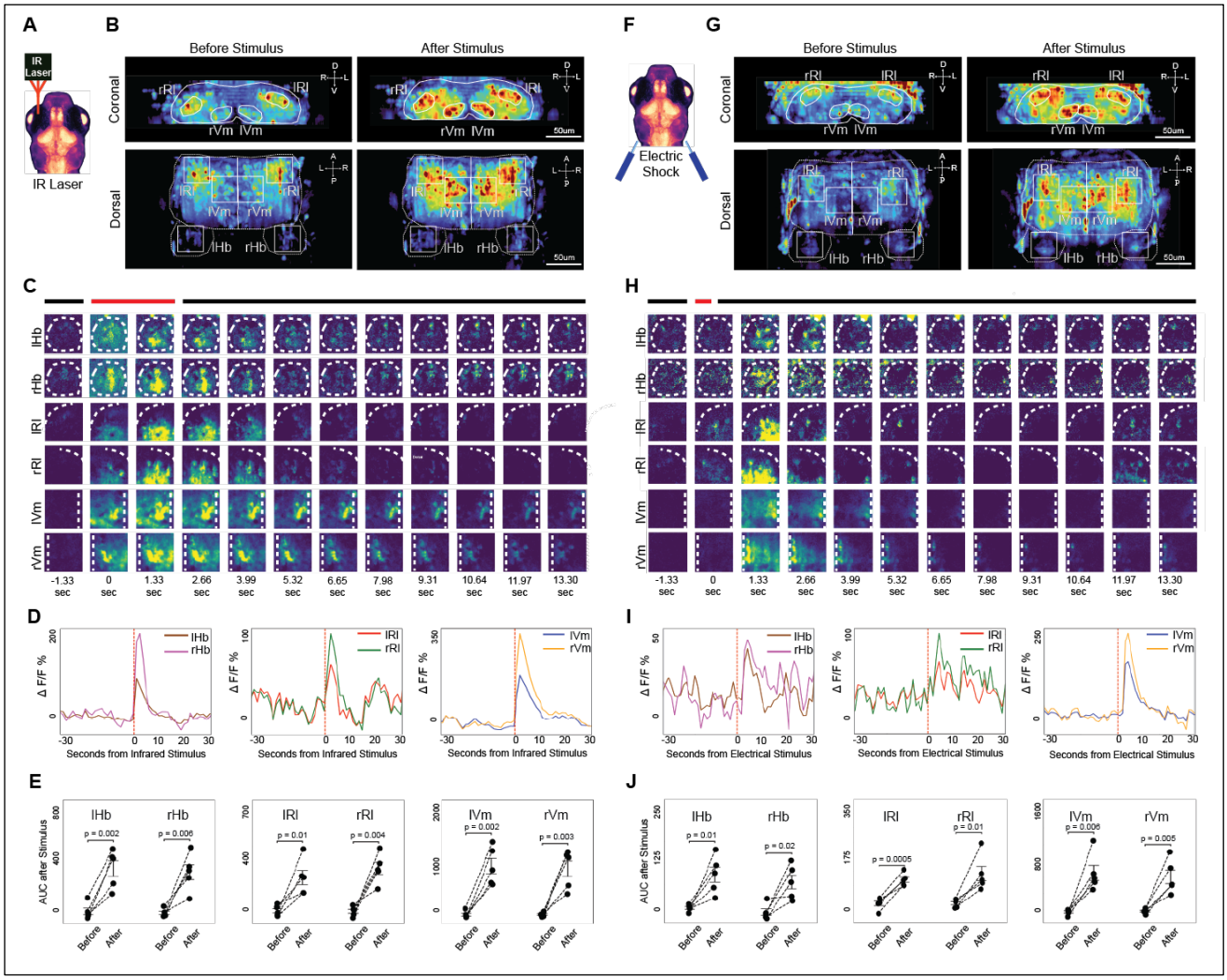

Figure 1 Neuronal activation in response to IR heating and electric shock

(**A**) Experimental setup with an infrared (IR) laser aimed at a 7 dpf larval zebrafish to deliver a heat stimulus.

(**B**) Heat maps of GCaMP fluorescence from a representative fish averaged over 5 presentations of IR heating. Enhanced activity is displayed in rostrolateral (lRL, rRL) and ventromedial (lVm, rVm) areas of the pallium, and habenula (lHb, rHb) in coronal and dorsal views post-laser exposure.

(**C**) Timelapse of average neuronal activation in response to exposure to the IR laser in the forebrain of a representative zebrafish. Each square corresponds to an area outlined in the dorsal view in (B). Brain regions where activity measurements were taken are outlined with dotted lines. Background activity was subtracted from all images.

(**D**) Region-specific ΔF/F activity traces from a representative fish, averaged across 5 trials, display pronounced increases in all measured areas following IR laser exposure.

(**E**) Analysis of the area under the curve (AUC; 5 frames, 6.65 seconds) ΔF/F for each fish for each brain region outlined in (**B**, **C**). Mean ± SEM for n=5 fish.

(**F**) Illustration of electric shock delivery to a 7 dpf larval zebrafish.

(**G**) Heat maps from a representative fish averaged over 5 presentations of electric shock. Enhanced activity is displayed in rostrolateral (lRL, rRL) and ventromedial (lVm, rVm) areas of the pallium, and habenula (lHb, rHb) in coronal and dorsal views post-laser exposure.

(**H**) Timelapse of average neuronal activation in response to exposure to electric shock in the forebrain of a representative zebrafish. Each square corresponds to an area outlined in the dorsal view in (G). Brain regions where activity measurements were taken are outlined with dotted lines. Background activity was subtracted from all images.

(**I**) Region-specific ΔF/F activity traces from a representative fish, averaged across 5 trials, display pronounced increases in all measured areas following electric shock.

(**J**) Analysis of the area under the curve (AUC; 4 frames, 5.32 seconds) ΔF/F for each fish for each brain region outlined in (G, H). Mean ± SEM for n=5 fish.

One-tailed t-test was used for all statistical comparisons.

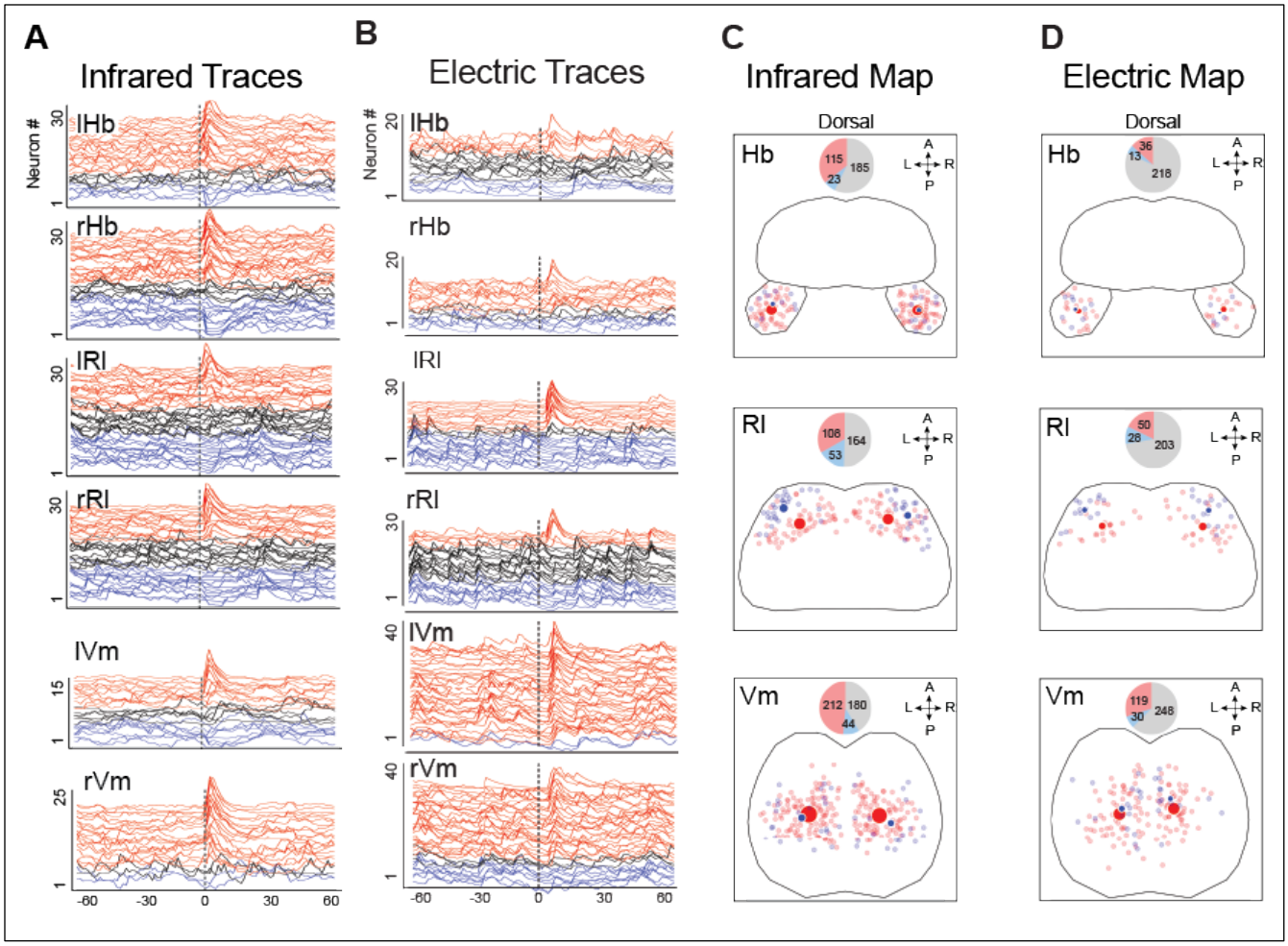

Figure 2. Response of neuronal components to noxious heat stimuli and electric shock.

(A) Neuronal component ΔF/F traces from an example fish as determined by CaImAn reveal a diverse response upon IR stimulation at the vertical dotted line. Red denotes activation (increase in activity ≥ 50% of background DF/F); blue, inhibition (decrease in activity ≤ -50% of background DF/F); Black, neither. Order is determined by z-score (μ/σ), which is a measure of the magnitude and consistency of the response.

(**B**) Neuronal component ΔF/F traces as in (A) in response to electric shock at the vertical dotted line.

(**C**) Locations of activated (small red dots) and inhibited (small blue dots) neuronal components in response to heating with an IR laser for all fish tested. Large dots are centers of mass of corresponding neuronal components. Pie graphs (inset) show the number of activated (red) inhibited (blue), and unresponsive (grey) neuronal components.

(**D**) Same as (C), but for neurons that respond to electric shock

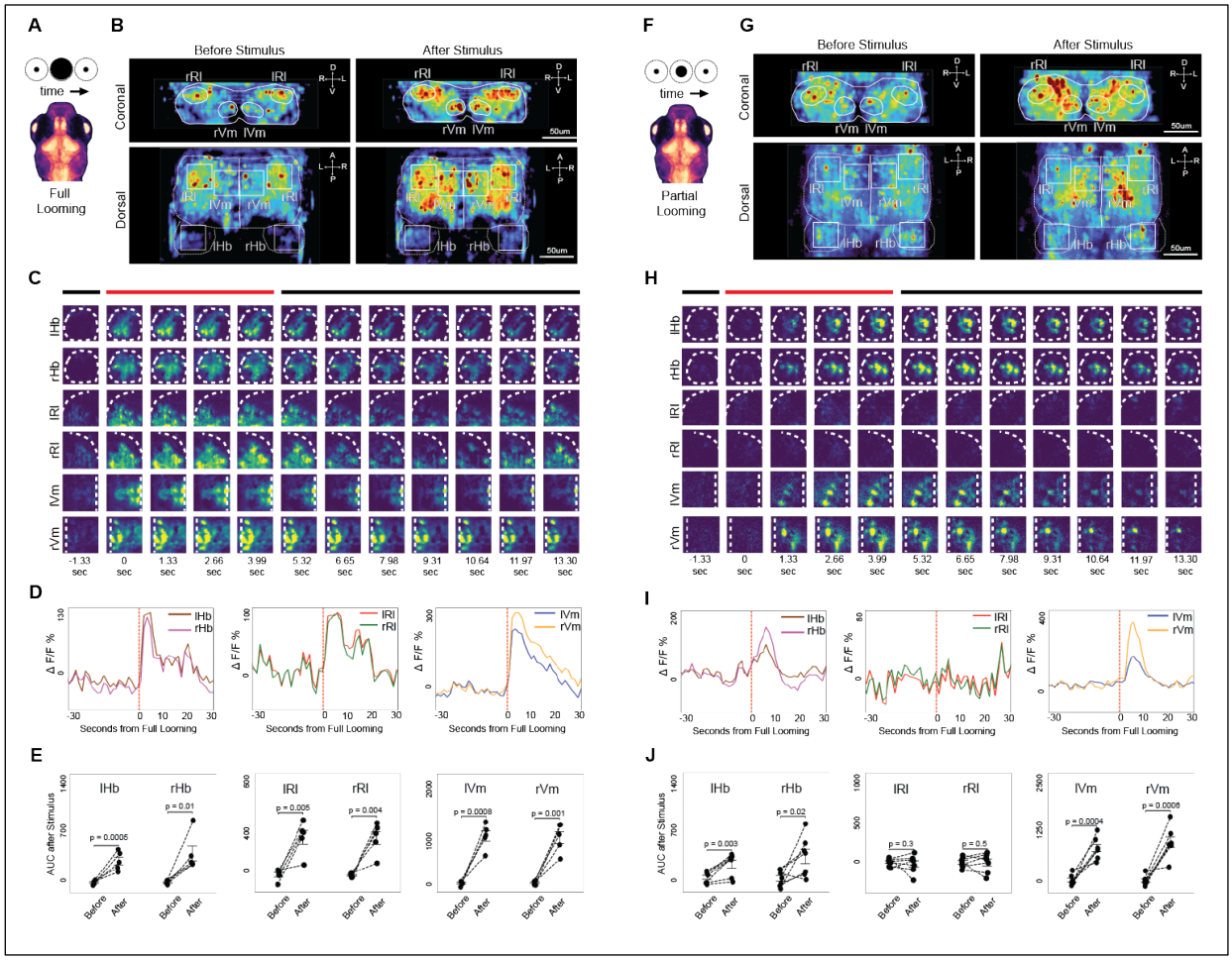

Figure 3. Neuronal activation in response to full and partial looming stimuli.

(**A**) Schematic of a 7 dpf zebrafish subjected to a full-looming disc stimulus.

(**B**) Neuronal activation in a representative zebrafish immediately before and after a full looming stimulus, averaged over 5 presentations, shows an increase in average activity across all brain areas previously found to be activated by noxious stimuli (rHb, lHb, rRl, lRl, rVm, lVm).

(**C**) Timelapse of heatmaps for the six areas outlined in (B) shows an abrupt increase in activity that commences with the full-looming stimulus.

(**D**) Region-specific ΔF/F activity traces from a representative fish, averaged across 5 trials, display pronounced increases in all measured areas following IR laser exposure.

(**E**) Mean increase above background ± SEM for ΔF/F A.U.C. for 5 frames, 6.65 seconds for each fish for each brain region outlined in (B)

(**F**) Schematic of a 7 dpf zebrafish subjected to a partial-looming disc stimulus.

(**G**) Neuronal activation in a representative zebrafish immediately before and after a partial looming stimulus, averaged over 3 presentations.

(**H**) Time-lapse of heatmaps for the six areas outlined in (B) shows an increase in activity in the Hb and Vm regions, but no significant change in activity in the Rl region. Activity in Hb and Vm was sustained for over 10 seconds.

(**I**) Region-specific ΔF/F and activity traces from a representative fish, averaged across 3 trials, display significant activity increases in Hb and Vm, but not in Rl, in response to the partial looming stimulus.

(**J**) Mean increase above background ± SEM for ΔF/F after the partial-looming stimulus (12 frames, ~16 seconds).

All statistical comparisons made with one-tailed t-test.

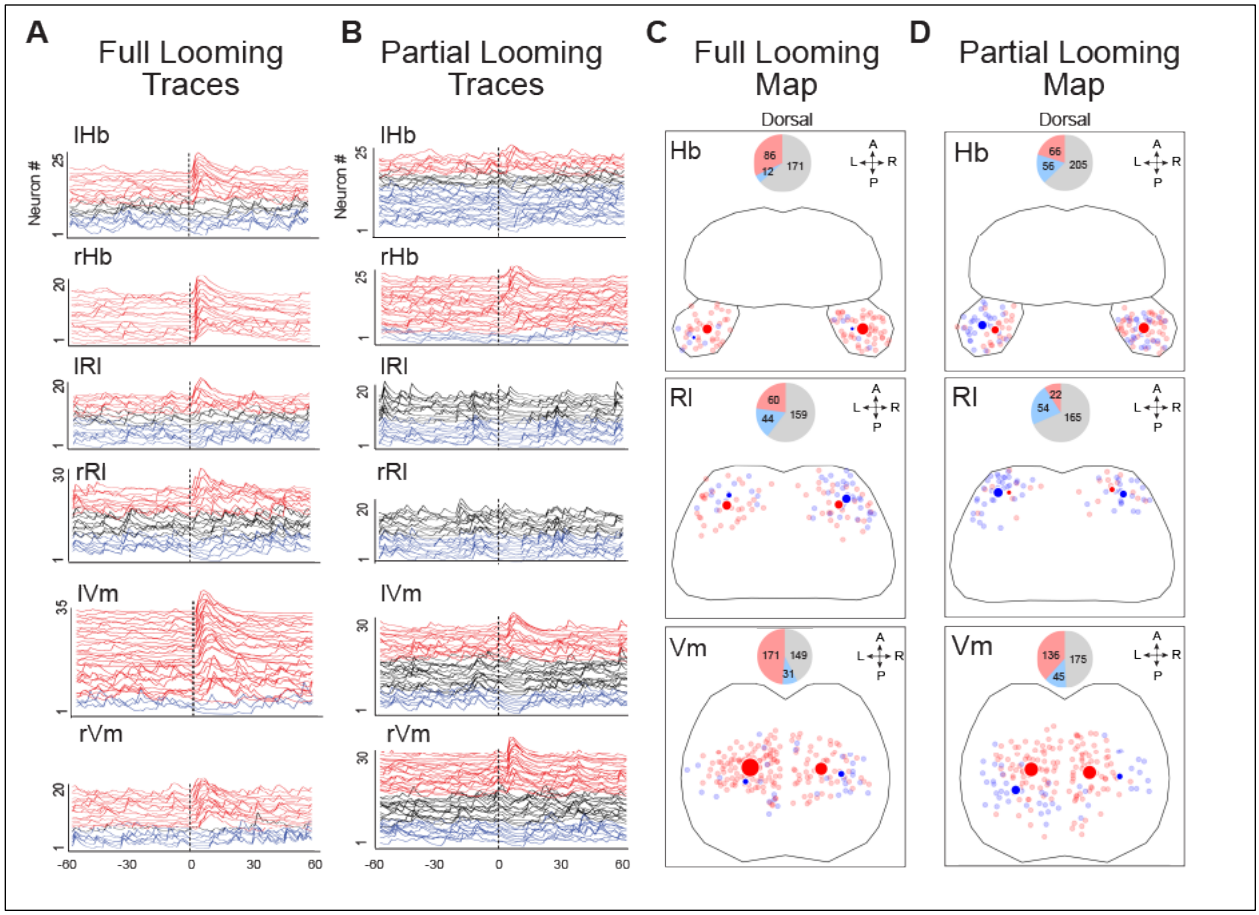

Figure 4. Response of neuronal components to full and partial looming stimuli.

(**A**) Neuronal component ΔF/F traces for an exemplary fish in response to a full looming stimulus at the vertical dotted line, averaged over 5 presentations. Red denotes activation (increase in activity ≥ 50% of background ΔF/F); blue, inhibition (decrease in activity ≤ -50% of background ΔF/F); black, neither. Order is determined by z-score (μ/σ), which is a measure of the magnitude and consistency of the response.

(**B**) Neuronal activity as in (A) in response to a partial looming stimulus averaged over 3 presentations in an exemplary fish. Activated and inhibited traces are seen in Hb and Vm, but not in Rl.

(**C**) Locations of neurons that are activated (small red dots) and inhibited (small blue dots) in response to a full looming stimulus for all fish tested. Large dots are centers of mass of corresponding neuronal components. Pie graphs (inset) show the number of activated (red), inhibited (blue), and unresponsive (grey) neuronal components.

(**D**) Same as (C) in response to a partial looming stimulus for all fish tested.

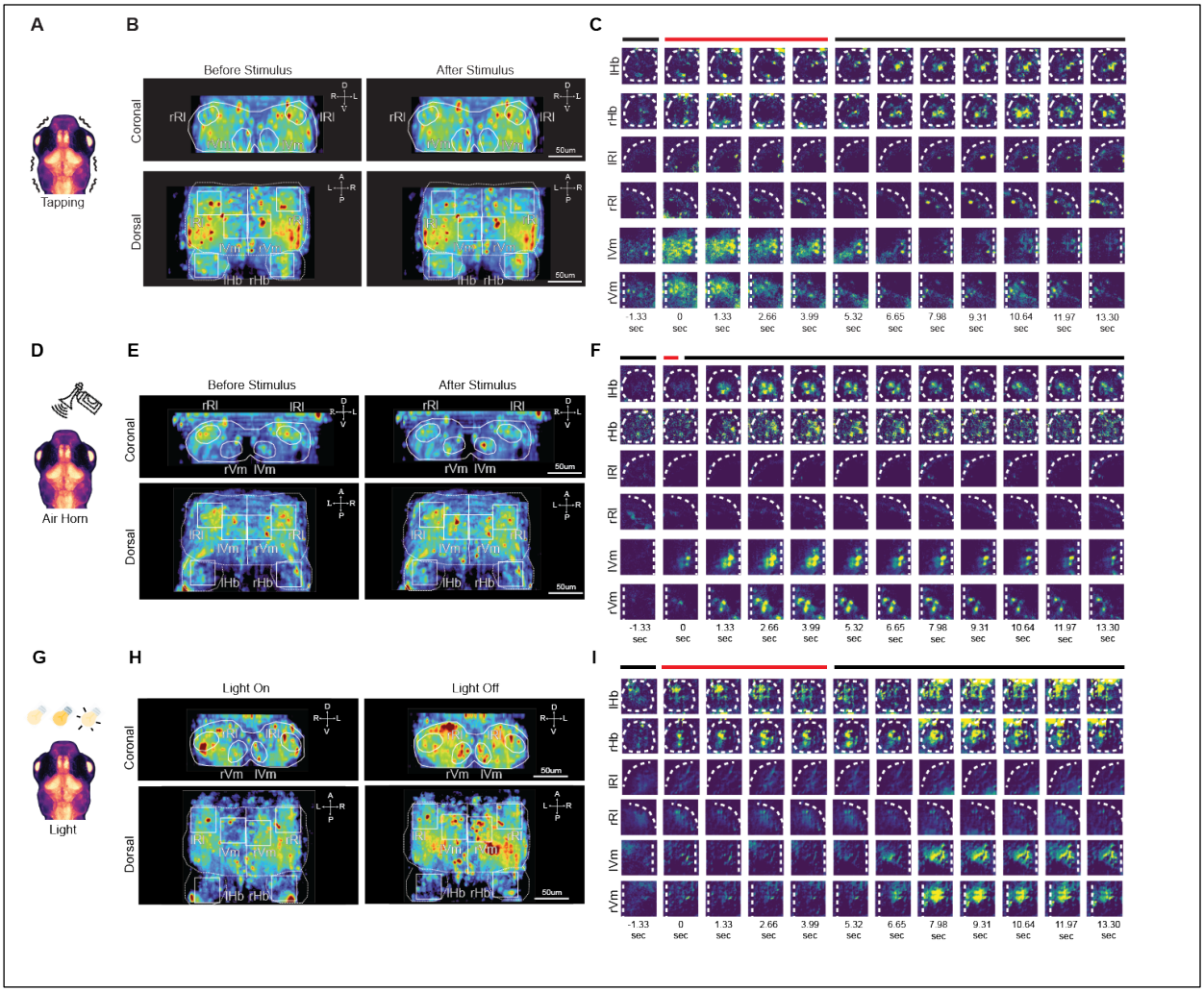

Figure 5. Neuronal activation in response to vibration, a loud noise, and light.

(**A**) Schematic of a 7 dpf zebrafish subjected to vibration.

(**B**) Neuronal activation in a representative zebrafish immediately before and after a vibration stimulus, averaged over 5 presentations, shows an increase in average activity across Hb and Vm, but not Rl.

(**C**) Timelapse of heatmaps for areas outlined in (B) show an increase in activity that commences with the initiation of tapping and grows until 14 s after cessation of tapping in Hb. In Vm the activity increases during the tapping stimulus and decreases abruptly after cessation. There is no increase in activity in Rl.

(**D**) Schematic of a 7 dpf zebrafish subjected to the blast of an air horn.

(**E**) Neuronal activation in a representative zebrafish immediately before and after an air horn blast, averaged over 5 presentations, shows an increase in average activity across Hb and Vm, but not Rl.

(**F**) Timelapse of heatmaps for areas outlined in (E) show an increase in activity that commences with the onset of the loud noise in Hb and Vm and lasts for over 10 s. There is no increase in activity in RI.

(**G**) Schematic of a 7 dpf zebrafish that is first equilibrated to darkness, then exposed to light for 4 s and then returned to darkness.

(**H**) Neuronal activation in a representative zebrafish immediately before and after transitioning from light to darkness, averaged over 5 presentations shows an increase in average activity across Hb and Vm, but not RI.

(**I**) Timelapse of heatmaps for areas outlined in (H) shows an increase in activity in Hb and Vm that commences ~ 2 s after the onset of darkness and lasts for over 5 s. There is no increase in activity in RI.

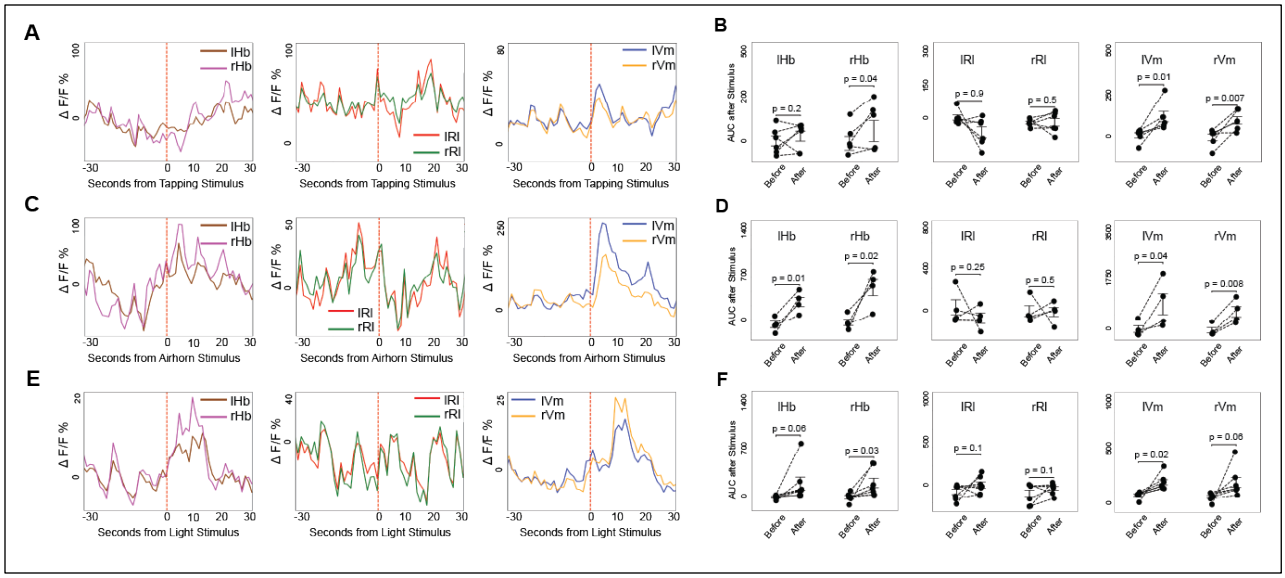

Figure 6 Response of total ΔF/F within different regions to vibration, a loud noise, and light

(**A**) Average ΔF/F activity traces within specific regions from a representative fish, averaged across 5 trials in response to a tapping stimulus.

(**B**) Activity rates for 6 fish before and after the tapping stimulus. Significant increases in activity were seen in rHb, lVm, and rVm, but not in lHb and Rl.

(**C**) Average ΔF/F activity traces within specific regions (AUC; 7 frames, 9.31 seconds) from a representative fish, averaged across 5 trials in response to a blast from an airhorn.

(**D**) Responses to a blast from an airhorn from 4 fish. Significant increases in activity were seen in HB and Vm, but not in Rl.

(**E**) Average ΔF/F activity traces within specific regions from a representative fish, averaged across 5 trials in response to a light-to-dark transition.

(**F**) Responses to a light-to-dark transition from 6 fish. Significant increases in activity were seen in rHB and lVm, but not in lHb, rVm, and Rl.

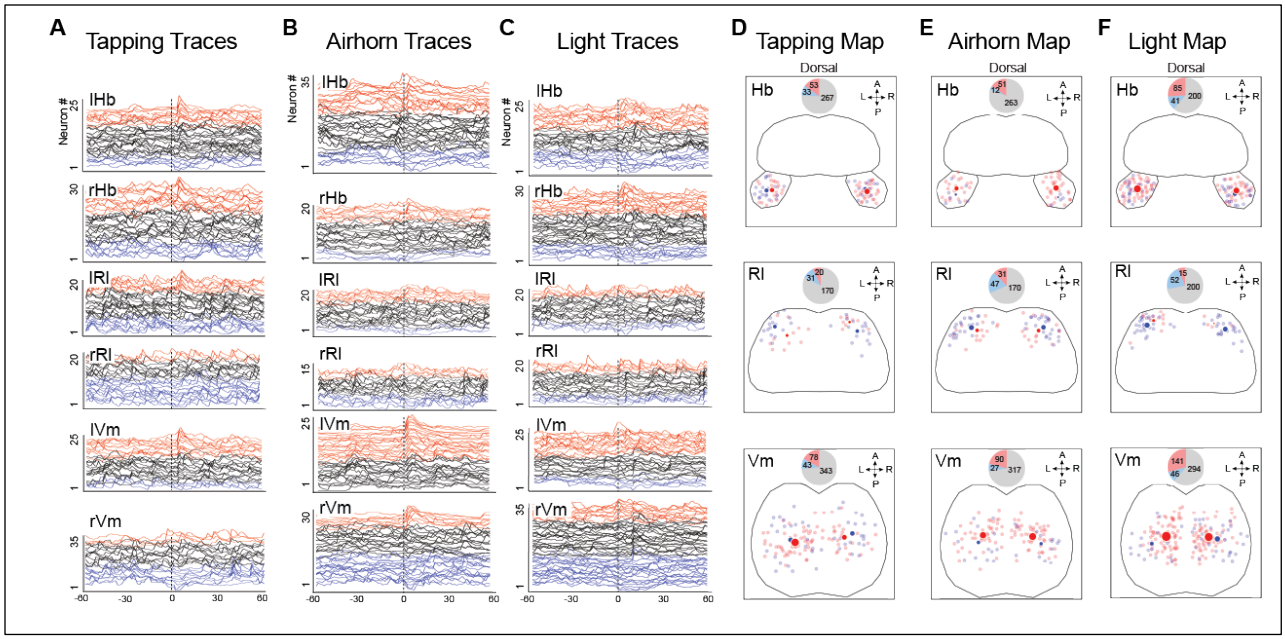

Figure 7 Response of neuronal components to vibration, a loud noise, and light

(**A**) Neuronal component ΔF/F traces of a representative fish in response to tapping at the vertical dotted line. Red denotes activation (increase in activity ≥ 50% of background ΔF/F); blue, inhibition (decrease in activity ≤ -50% of background ΔF/F); black, neither. Order is determined by z-score (μ/σ), which measures the magnitude and consistency of the response. In Hb and Vm, the responses of neuronal components to all three stimuli tend to be better defined than those in Rl.

(**B, C**) Neuronal component ΔF/F traces as in (A), but in response to the blast of an airhorn (B) or a transition from light to dark (C) at the vertical dotted line.

(**D-F**) Locations of neuronal components in Hb, Rl, and Vm. Small puncta mark locations where neuronal components respond by increasing (red) or decreasing (blue) activity in response to tapping (D), a blast from an airhorn (E) or a transition from light to dark (F). Large dots represent centers of mass of corresponding neuronal components. Pie graphs (inset) show the number of activated (red), inhibited (blue), and unresponsive (grey) neuronal components. Note that in Rl, inhibited neurons outnumber activated neurons, whereas in Hb and Vm, the proportion of activated components are roughly equal to or greater than that of inhibited components.

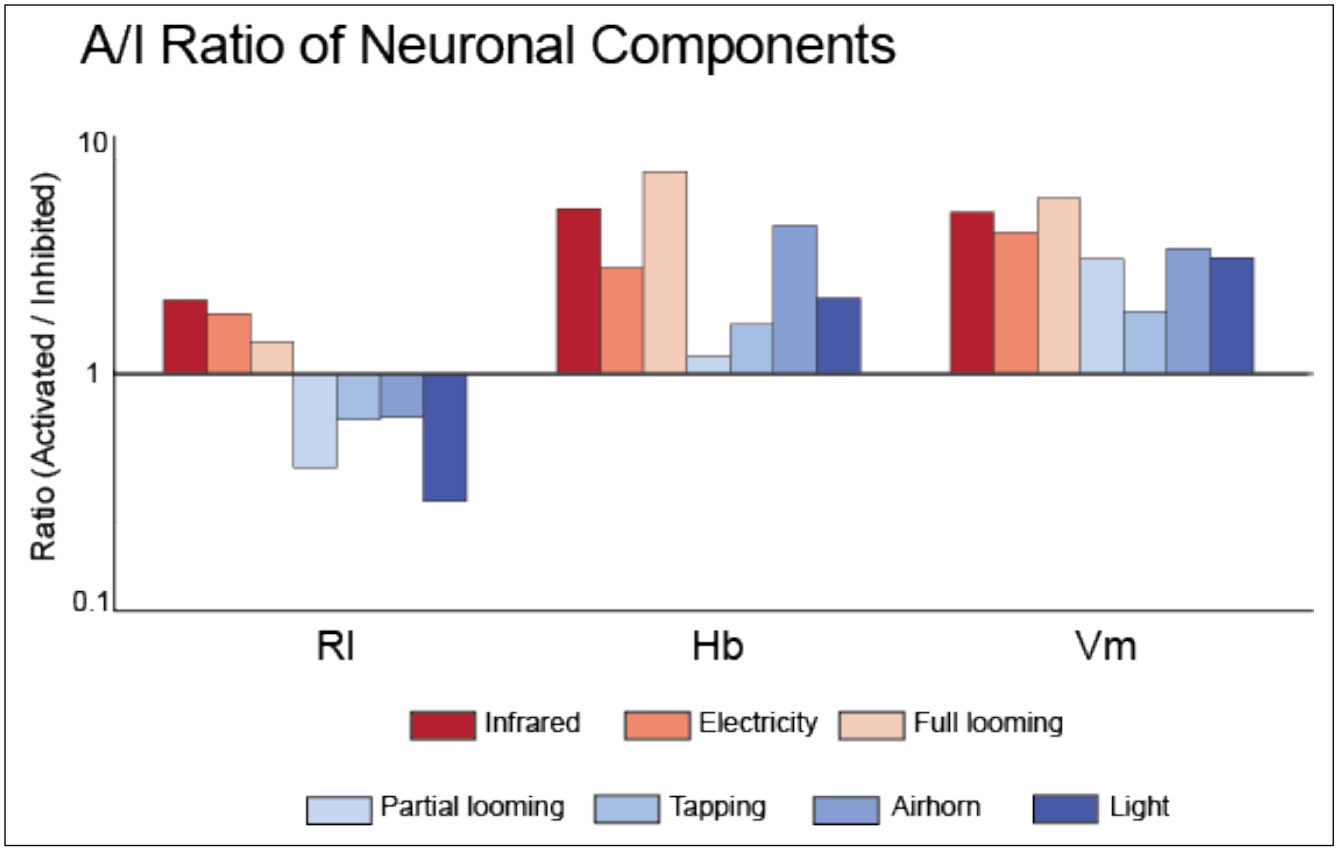

Figure 8 RI is activated by highly threatening stimuli but not by mildly threatening stimuli.

The ratio of activated to inhibited neuronal components (A/I) in RI is greater than 1 for highly threatening stimuli but less than 1 for mildly aversive stimuli. In contrast, in Hb and Vm, the A/I ration is greater than one for all aversive stimuli.

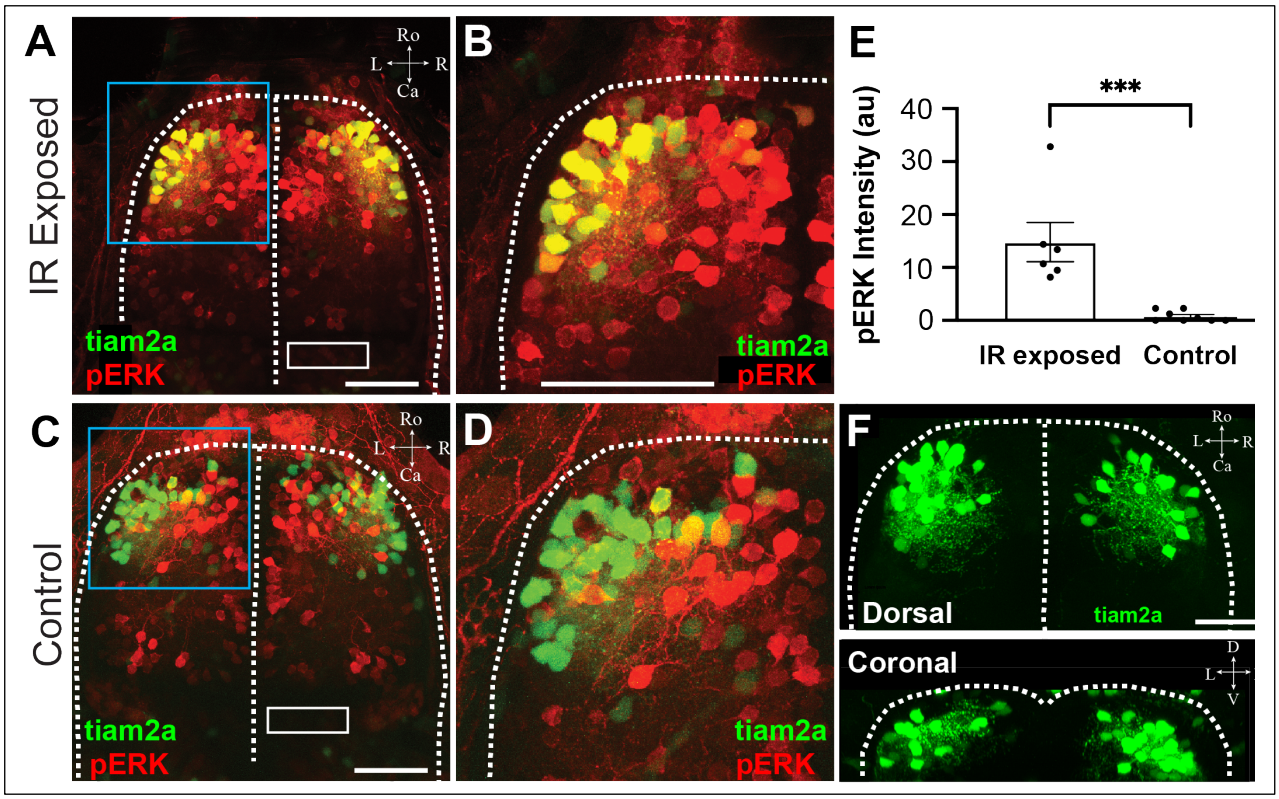

Figure 9 Cells expressing tiam2a become active when exposed to IR heating.

(**A**) 7 dpf Tg[tiam2a:GFP] larval zebrafish exposed 10 times to heating with an IR laser and then immunostained for pERK to label active neurons. Virtually all GFP-positive neurons were co-labeled with pERK, suggesting that Tiam2a-positive cells are activated by a painful stimulus.

(**B**) Close-up of the area bordered by the blue rectangle in (A).

(**C**) 7 dpf Tg[tiam2a:GFP] larval zebrafish control that was not exposed to heating showed very little overlap between GFP labeling and labeling for pERK.

(**D**) Closeup of the area bordered by the blue rectangle in (C).

(**E**) Average intensity of pERK immunostaining in Tiam2a+ cells, with background (measured in the white rectangle in (A)) subtracted, for fish exposed to IR heating (n = 6) and control fish (n = 8). Significantly more labeling was found in fish exposed to heating (P = 0.0009, t-test) vs. in control fish.

(**F**) Tg[tiam2a:GFP] fish showing cell bodies concentrated in the rostrolateral area and local axonal connections.